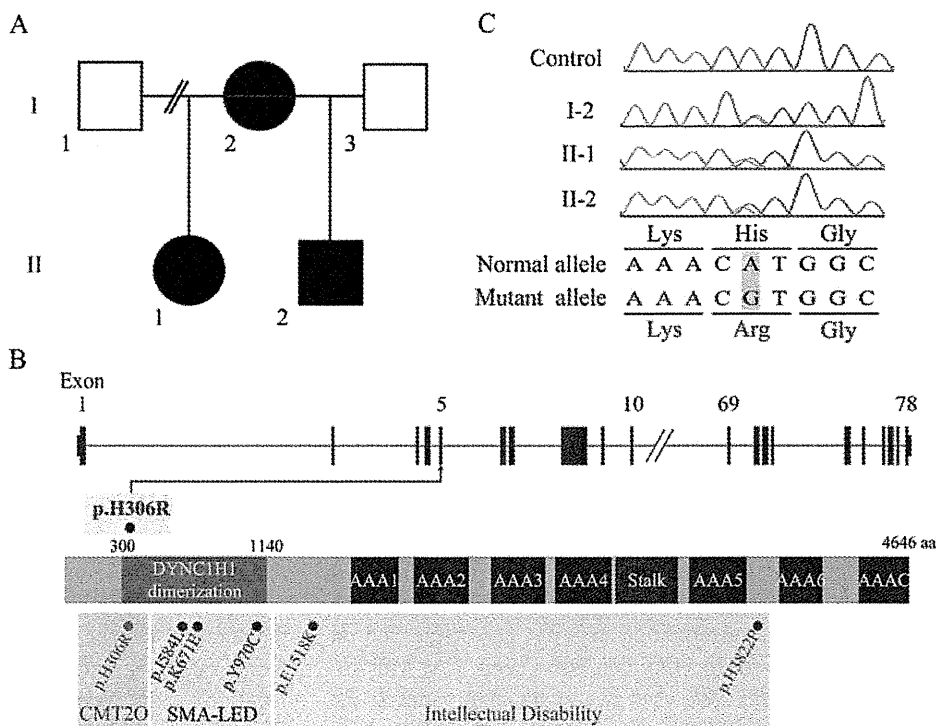


Fig. 2 Histological study. Hematoxylin–eosin staining (*upper*) and ATPase staining (pH=4.6, *lower*) of the quadriceps femoris muscle of patient II-1. The scale bar indicates 100 μm in length

SeattleSeq Annotation website (<http://gvs.gs.washington.edu/SeattleSeqAnnotation/>).

Fig. 3 Genetic study. **a** Familial pedigree. **b** The gene structure of *DYNC1H1* with the mutation [p.H306R (c.917A>G)] (*upper*), the protein structure with functional domains (*middle*), and reported mutations corresponding to respective diseases (*lower*). AAA ATPase domains (AAA 1 to 6), AAAC unrelated seventh domain. **c** Sequences of a control and the family members are displayed. Heterozygous mutations are observed in patients I-2, II-1, and II-2



Priority scheme and capillary sequencing

We adopted a prioritization scheme used in recent studies to identify the pathogenic mutation [5–7]. Called variants found by each informatics method filtered into unregistered variants (excluding registered dbSNP131 and 1,000 genomes), overlapping variants called in common by NextGENe and MAQ, nonsynonymous changes (NS), splice site mutations (± 2 bp from the exon–intron junctions) (SS), small insertions or deletions (indels), and overlapping variants called in II-1 and II-2 were checked, and variants found in our 33 in-house exomes derived from 19 healthy individuals and 14 individuals with unrelated diseases were excluded (Table 1). An online human genome mutation database (HGMD, <https://portal.biobase-international.com/hgmd/pro/start.php>) was referred to as a reference for disease-causing mutations. The variants were confirmed as true positives by Sanger sequencing of polymerase chain reaction products amplified using genomic DNA as a template. Sanger sequencing was performed on an ABI3500XL or ABI3100 autosequencer (Life Technologies, Carlsbad, CA). Sequencing data were analyzed using Sequencer software (Gene Codes Corporation, Ann Arbor, MI).

A total of 177 Japanese control samples (354 alleles) were checked by high-resolution melting analysis using a LightCycler 480 (Roche Diagnostics, Otsu, Japan) to see the variant frequency. The reaction was performed in 10 μl containing 10 ng of genomic DNA, 0.2 mM dNTPs,

Table 1 Variant priority scheme of exome sequencing data

	Half sister		Half brother	
	NextGENe	MAQ (SeattleSeq)	NextGENe	MAQ (SeattleSeq)
Total variants called	73,966	174,757	73,370	163,707
Autosomal+chr X	71,522	174,165	70,068	163,013
Unknown SNP variants (dbSNP, 1,000 genomes)	11,132	21,284	10,857	19,858
Overlap of NextGENe and MAQ		1,598		1,482
NS/SS/I		426		411
Overlapping in half sibs			135	
Unknown variants (in-house database)			62	

MAQs were annotated using SeattleSeq annotation. The annotation includes gene names, dbSNP rs IDs, and SNP functions (e.g., missense), protein positions and amino acid changes. *NS* nonsynonymous, *SS* splice site (± 2 bp), *I* indels

0.125 U of ExTaq (Takara Bio, Inc., Otsu, Japan), $1\times$ buffer, and $1.5\ \mu\text{M}$ SYTO9 (Invitrogen, Carlsbad, CA).

Results

Approximately 9.8 and 9.5 Gb of sequence data were generated for II-1 and II-2, respectively. This approach resulted in more than 85.8 % (II-1) and 86.5 % (II-2) of the target regions being covered by ten reads or more. Two informatics methods identified 62 potentially pathogenic changes (Table 1). We found a missense mutation [p.H306R (c.917A>G)] in *DYNC1H1* from among 62 variants using the HGMD as a reference; this mutation has been reported as a causative mutation for CMT disease [2]. The heterozygous missense mutation was confirmed in I-2, II-1, and II-2 (Fig. 3b). This missense mutation was not found in 177 control samples.

Discussion

The identical *DYNC1H1* mutation (p.H306R) found in a large pedigree with axonal type of CMT disease was detected by exome sequencing in a family with a unique form of quadriceps-dominant neurogenic muscular atrophy [2]. Three members of the family demonstrated very similar clinical features, which were distinct from CMT disease. The most striking feature was a unique distribution of muscle involvement. The quadriceps femoris muscle was almost selectively involved in the early course of the disease, and the proximal lower limb was predominantly involved throughout the disease course. Recently, three other missense mutations were detected in families with SMA-LED. Clinical features of the current family are essentially consistent with those of SMA-LED, hallmarks of which are early childhood onset of proximal leg weakness with muscle atrophy and nonlength-dependent motor neuron disease without sensory involvement [3]. Nonprogressive clinical

course despite early childhood onset as in our family should be another hallmark of SMA-LED. These cumulative data clearly indicate that *DYNC1H1* plays an essential role in maintenance of spinal motor neurons and their axon.

Thus far, four missense mutations (p.H306R, p.I584L, p.K671E, p.Y970C) identified in human cases of CMT or SMA-LED are located in the same tail domain for *DYNC1H1* dimerization. It is of note that three missense mutations (p.F580Y, p.G1042A, p.T1057C) found in mouse models are also located in the tail domain [8–10]. These mice involve not only spinal motor neurons but also sensory and cortical neurons. The tail domain is thought to be essential for dimerization of dynein heavy chains, and thus, missense mutations in the tail domain may disrupt function of dynein complex formation in a dominant negative manner. Two distinct de novo mutations (p.E1518K, p.H3822P) identified in patients with severe intellectual disability and variable neuronal migration defects were located outside of the tail domain. These patients also showed possible peripheral nerve involvement, but formal neurophysiological investigation was not available. Since mice with *Dync1h1* abnormality show broad central nervous system involvement, *DNYC1H1* is likely to cause a wide range of neuronal migration disorders.

CMT disease with the p.H306R mutation has been designated as CMT2O (OMIM 614228). Most members of the pedigree with p.H306R reported by Weedon et al. demonstrated distal dominant muscle weakness, while one patient showed proximal lower limb-dominant muscle atrophy as in our family [2]. Therefore, the same missense mutation in the tail domain could cause CMT2O phenotype and SMA-LED phenotype even within the same pedigree. It is hard to explain the underlying mechanism of pleiotropic effects of the mutation. Further studies are absolutely necessary to elucidate phenotype–genotype correlation and pleiotropic mutational consequences.

Acknowledgments We would like to thank the family for their participation in this study. This work was supported by research grants from the Ministry of Health, Labour and Welfare (H.S., N. Miyake, and

N. Matsumoto); a Grant-in-Aid for Scientific Research from the Japan Society for the Promotion of Science (N. Miyake and N. Matsumoto); a grant from the Japan Science and Technology Agency (N. Matsumoto), the Strategic Research Program for Brain Sciences (N. Matsumoto); a Grant-in-Aid for Scientific Research on Innovative Areas (Foundation of Synapse and Neurocircuit Pathology) from the Ministry of Education, Culture, Sports, Science and Technology of Japan (N. Matsumoto); a research grant from Naito Foundation (N. Matsumoto); and research grants from Takeda Science Foundation (N. Miyake and N. Matsumoto). This work was performed at the Advanced Medical Research Center, Yokohama City University, Japan.

References

- Pfister KK, Shah PR, Hummerich H, Russ A, Cotton J, Annuar AA, King SM, Fisher EM (2006) Genetic analysis of the cytoplasmic dynein subunit families. *PLoS Genet* 2(1):e1. doi:10.1371/journal.pgen.0020001
- Weedon MN, Hastings R, Caswell R, Xie W, Paszkiewicz K, Antoniadis T, Williams M, King C, Greenhalgh L, Newbury-Ecob R, Ellard S (2011) Exome sequencing identifies a *DYNC1H1* mutation in a large pedigree with dominant axonal Charcot-Marie-Tooth disease. *Am J Hum Genet* 89(2):308–312. doi:10.1016/j.ajhg.2011.07.002
- Harms MB, Ori-McKenney KM, Scoto M, Tuck EP, Bell S, Ma D, Masi S, Allred P, Al-Lozi M, Reilly MM, Miller LJ, Jani-Acsadi A, Pestronk A, Shy ME, Muntoni F, Vallee RB, Baloh RH (2012) Mutations in the tail domain of *DYNC1H1* cause dominant spinal muscular atrophy. *Neurology* 78(22):1714–1720. doi:10.1212/WNL.0b013e3182556c05
- Willemsen MH, Vissers LE, Willemsen MA, van Bon BW, Kroes T, de Ligt J, de Vries BB, Schoots J, Lugtenberg D, Hamel BC, van Bokhoven H, Brunner HG, Veltman JA, Kleefstra T (2012) Mutations in *DYNC1H1* cause severe intellectual disability with neuronal migration defects. *J Med Genet* 49(3):179–183. doi:10.1136/jmedgenet-2011-100542
- Tsurusaki Y, Okamoto N, Suzuki Y, Doi H, Saitu H, Miyake N, Matsumoto N (2011) Exome sequencing of two patients in a family with atypical X-linked leukodystrophy. *Clin Genet* 80(2):161–166. doi:10.1111/j.1399-0004.2011.01721.x
- Saitu H, Osaka H, Sasaki M, Takahashi J, Hamada K, Yamashita A, Shibayama H, Shiina M, Kondo Y, Nishiyama K, Tsurusaki Y, Miyake N, Doi H, Ogata K, Inoue K, Matsumoto N (2011) Mutations in *POLR3A* and *POLR3B* encoding RNA polymerase III subunits cause an autosomal-recessive hypomyelinating leukoencephalopathy. *Am J Hum Genet* 89(5):644–651. doi:10.1016/j.ajhg.2011.10.003
- Doi H, Yoshida K, Yasuda T, Fukuda M, Fukuda Y, Morita H, Ikeda S, Kato R, Tsurusaki Y, Miyake N, Saitu H, Sakai H, Miyatake S, Shiina M, Nukina N, Koyano S, Tsuji S, Kuroiwa Y, Matsumoto N (2011) Exome sequencing reveals a homozygous *SYT14* mutation in adult-onset, autosomal-recessive spinocerebellar ataxia with psychomotor retardation. *Am J Hum Genet* 89(2):320–327. doi:10.1016/j.ajhg.2011.07.012
- Hafezparast M, Klocke R, Ruhrberg C, Marquardt A, Ahmad-Annar A, Bowen S, Lalli G, Witherden AS, Hummerich H, Nicholson S, Morgan PJ, Oozageer R, Priestley JV, Averill S, King VR, Ball S, Peters J, Toda T, Yamamoto A, Hiraoka Y, Augustin M, Korthaus D, Wattler S, Wabnitz P, Dickneite C, Lampel S, Boehme F, Peraus G, Popp A, Rudelius M, Schlegel J, Fuchs H, Hrabe de Angelis M, Schiavo G, Shima DT, Russ AP, Stumm G, Martin JE, Fisher EM (2003) Mutations in dynein link motor neuron degeneration to defects in retrograde transport. *Science* 300(5620):808–812. doi:10.1126/science.1083129
- Chen XJ, Levedakou EN, Millen KJ, Wollmann RL, Soliven B, Popko B (2007) Proprioceptive sensory neuropathy in mice with a mutation in the cytoplasmic dynein heavy chain 1 gene. *J Neurosci* 27(52):14515–14524. doi:10.1523/JNEUROSCI.4338-07.2007
- Ori-McKenney KM, Vallee RB (2011) Neuronal migration defects in the *Loa* dynein mutant mouse. *Neural Dev* 6:26. doi:10.1186/1749-8104-6-26

SHORT COMMUNICATION

The diagnostic utility of exome sequencing in Joubert syndrome and related disorders

Yoshinori Tsurusaki¹, Yasuko Kobayashi², Masataka Hisano³, Shuichi Ito⁴, Hiroshi Doi¹, Mitsuko Nakashima¹, Hiroto Saito¹, Naomichi Matsumoto¹ and Noriko Miyake¹

Joubert syndrome (JS) and related disorders (JSRD) are autosomal recessive and X-linked disorders characterized by hypoplasia of the cerebellar vermis with a characteristic ‘molar tooth sign’ on brain imaging and accompanying neurological symptoms including episodic hyperpnoea, abnormal eye movements, ataxia and intellectual disability. JSRD are clinically and genetically heterogeneous, and, to date, a total of 17 causative genes are known. We applied whole-exome sequencing (WES) to five JSRD families and found mutations in all: either *CEP290*, *TMEM67* or *INPP5E* was mutated. Compared with conventional Sanger sequencing, WES appears to be advantageous with regard to speed and cost, supporting its potential utility in molecular diagnosis.

Journal of Human Genetics advance online publication, 4 October 2012; doi:10.1038/jhg.2012.117

Keywords: *CEP290*; exome sequencing; *INPP5E*; Joubert syndrome; molecular diagnosis; *TMEM67*

Joubert syndrome (JS) and related disorders (JSRD) are autosomal recessive and X-linked disorders characterized by hypoplasia of the cerebellar vermis with the characteristic neuroradiological ‘molar tooth sign’ and accompanying neurological symptoms including dysregulation of breathing pattern, ataxia and developmental delay. JSRD are classified into six subtypes: pure JS, JS with ocular defect, JS with renal defect, JS with oculorenal defects, JS with hepatic defect and JS with orofaciocigital defects.¹ To date, 17 causative genes have been identified in JSRD: *INPP5E*,² *TMEM216*,³ *AHII*,⁴ *NPHP1*,⁵ *CEP290*,⁶ *TMEM67*,⁷ *RPGRIPL*,⁸ *ARL13B*,⁹ *CC2D2A*,¹⁰ *OFD1*,¹¹ *TTC21B*,¹² *KIF7*,¹³ *TCTN1*,¹⁴ *TMEM237*,¹⁵ *CEP41*,¹⁶ *TMEM138*,¹⁷ and *C5ORF42*.¹⁸ Because of the clinical and genetic heterogeneity in JSRD, it can be very difficult to identify the causative mutations in individual cases.

We encountered five non-consanguineous Japanese families with JSRD (Figure 1a) and molar tooth sign was observed in all patients (Figures 1b–e, Supplementary Table 1). Peripheral blood samples were obtained from patients and their family members after written informed consent was given. To identify causative mutations, we performed whole-exome sequencing (WES) in five probands of the five families (one proband from each family). DNA was processed using the SureSelectXT Human All Exon 50 Mb library or V4 (51 Mb) library (Agilent Technologies, Santa Clara, CA, USA), and sequenced on a Genome Analyzer Iix sequencer (Illumina, San Diego, CA, USA) with 108 bp paired-end reads, or on a HiSeq2000 sequencer (Illumina) with 101 bp paired-end reads and 7 bp index reads.

Image analysis and base calling were performed by Illumina pipeline. Approximately 3.8–6.0 Gb of sequence data were mapped to the human reference genome (GRCh37.1/hg19) with Novoalign or Burrows-Wheeler Aligner. The mean depth of coverage was 55–125 reads, with 88–96% of all coding exons being covered by 5 × or more reads.

Out of all variants within exons and ± 20-bp intronic regions from the exon–intron boundaries, those registered in dbSNP135, 1000 Genomes and ESP5400 and located within the segmental duplications were removed. Homozygous or compound heterozygous variants of 17 JSRD causative genes were then picked up. In patients 1, 2, 3 and 4 whose DNA was captured by the SureSelectXT Human All Exon 50 Mb library, ~90% of the entire coding regions in 13 of 17 causative genes were covered by 5 × reads or more. In patient 5 captured by the V4 (51 Mb) library, >90% of the coding region was covered by 5 × reads or more (Supplementary Table 2), indicating that the V4 library offered superior coverage to the SureSelectXT library around the regions of the JSRD genes.

All patients from the five families possessed novel compound heterozygous mutations or a homozygous mutation in known genes later confirmed by Sanger sequencing (Figure 1a): c.1862G>A (p.R621Q)/c.700dupC (p.L234Pfs*56) in *INPP5E* (9q34.3) for family 1; c.5788A>T (p.K1930*)/c.6012-12A>T in *CEP290* (12q21.32) for family 2; c.329A>G (p.D110G)/c.2322 + 5delG in *TMEM67* (8q22.1) for family 3; homozygous c.6012-12A>T in *CEP290* for family 4; and c.214G>T (p.E72*)/c.6012-12A>T in *CEP290* for family 5. No other variants within 17 known genes have been identified after excluding

¹Department of Human Genetics, Yokohama City University Graduate School of Medicine, Yokohama, Japan; ²Department of Pediatrics, Gunma University Graduate School of Medicine, Maebashi, Japan; ³Department of Nephrology, Chiba Children’s Hospital, Chiba, Japan and ⁴National Center for Child Health and Development, Tokyo, Japan
Correspondence: Dr N Miyake, Department of Human Genetics, Yokohama City University Graduate School of Medicine, 3-9 Fukuura, Kanazawa-ku, Yokohama 236-0004, Japan.
E-mail: nmiyake@yokohama-cu.ac.jp

Received 31 July 2012; revised 3 September 2012; accepted 5 September 2012

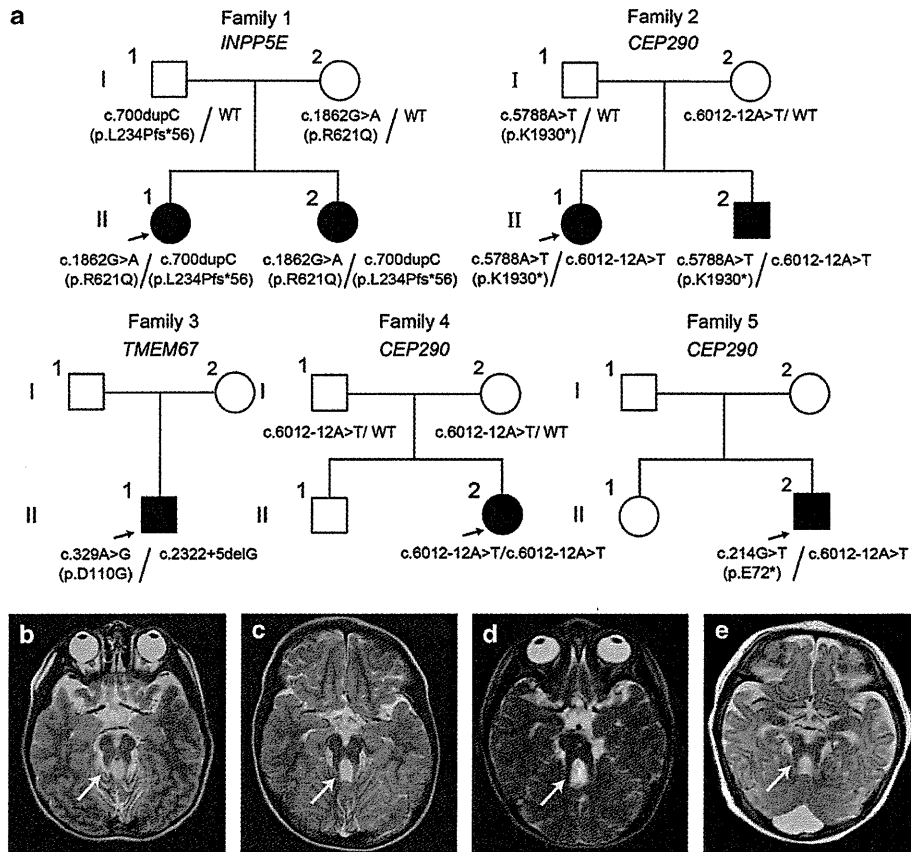


Figure 1 Familial pedigree and brain MRI of the patients. (a) JSRD families and mutations. (b) T2-weighted axial images of III-1, family 1. (c) T2-weighted axial images of III-2, family 1. (d) T2-weighted axial images of III-1, family 2. (e) T2-weighted axial images of III-2, family 2. The molar tooth sign is visible in all patients (arrowheads).

the variants of dbSNP135, 1000 Genomes and ESP5400. Clinical phenotypes caused by respective mutated genes are discussed in Supplementary text. In families 1, 2 and 4 in which parental samples were available, all parents were heterozygous carriers of one of the mutations. As parental samples were unavailable from families 3 and 5, we determined whether two mutations resided on different alleles by cloning a reverse transcriptase-PCR (RT-PCR) product amplified from total RNA of lymphoblastoid cells into a pCR4-TOPO vector (Life Technologies, Carlsbad, CA, USA) and sequencing. Each mutation was found in a different allele for both families (data not shown). Another variant, c.1894A>G (p.K632E) in *CEP290*, of family 2 was not found to be pathogenic based on web-based analyses such as SIFT, PolyPhen-2 and Mutation Taster (Supplementary Table 3). In families 2, 4 and 5 with a *CEP290* abnormality, c.6012-12A>T was shared. On the basis of our in-house 135 exome data, the allele frequency of the mutation was 1/270 allele (0.74%), indicating that it may be a rare variant in Japanese. The other mutations were not found in our in-house 135 exome data.

Splicing effects were examined in families 3 and 4. RT-PCR was performed on RNA from lymphoblastoid cells of family members using primers spanning exons 42/43 and 45/46 in family 4 and exons 20/21 and 24/25 in family 3 (sequence information available on request). In family 4, only an aberrant cDNA was detected in II-2, whereas the parents (I-1 and I-2) showed two different products including one wild-type, which was detected in a control

(Supplementary Figures 1a, b). Sequencing of the mutant product revealed a 57-bp insertion corresponding to the 3'-side of intron 43. As a result, a premature stop codon was introduced at intron 43. In family 3, RT-PCR detected a mutant cDNA in II-1 together with a wild-type product, which was detected in a control. Sequencing of the mutant product confirmed the skipping of exon 22, resulting in an in-frame 27 amino-acid deletion (Supplementary Figures 1c, d).

WES has proved a powerful tool for the identification of novel genes in genetic diseases. It also has tremendous potential for clinical diagnosis and is now being applied in the molecular diagnosis of single-gene disorders such as neurofibromatosis type 1, Marfan syndrome and multi-gene disorders such as retinitis pigmentosa.¹⁹ As shown here, WES would also be suitable for the diagnosis of JSRD, another multi-gene disorder. Though the read-coverage of the old version of SureSelect did not sufficiently collect genomic DNAs for four genes (*INPP5E*, *TMEM216*, *KIF7* and *TCTN1*), the performance of the V4 (51 Mb) library was satisfactory for all genes. Further, as exome capture technology is based on hybridization it can be refractory to homologous regions, so other methods such as multiplex PCR amplification and multiple microdroplet PCR technology could be useful in addition.

In conclusion, we were able to identify causative mutations in five non-consanguineous families with JSRD using WES. The diagnostic utility of WES is obvious, implying that WES or other next-generation sequencing technologies will be a main factor of molecular diagnosis.

ACKNOWLEDGEMENTS

We thank the patients and their families for their participation in this study. This work was supported by research grants from the Ministry of Health, Labor and Welfare (HS, N Matsumoto, N Miyake), the Japan Science and Technology Agency (N Matsumoto), the Strategic Research Program for Brain Sciences (N Matsumoto) and a Grant-in-Aid for Scientific Research on Innovative Areas-(Transcription cycle)-from the Ministry of Education, Culture, Sports, Science and Technology of Japan (N Matsumoto), a Grant-in-Aid for Scientific Research from Japan Society for the Promotion of Science (N Matsumoto), a Grant-in-Aid for Young Scientist from Japan Society for the Promotion of Science (HS, N Miyake) and a grant from the Takeda Science Foundation (N Matsumoto, N Miyake).

Web Resources: The URLs for data presented herein are as follows:

Novoalign, <http://www.novocraft.com/main/index.php>: Burrows-Wheeler Aligner, <http://bio-bwa.sourceforge.net/>: SIFT, <http://sift.jcvi.org/>: PolyPhen-2, <http://genetics.bwh.harvard.edu/pph2/>: Mutation Taster, <http://neurocore.charite.de/MutationTaster/>

- 1 Brancati, F., Dallapiccola, B. & Valente, E. M. Joubert Syndrome and related disorders. *Orphanet. J. Rare Dis.* **5**, 20 (2010).
- 2 Bielas, S. L., Silhavy, J. L., Brancati, F., Kisseleva, M. V., Al-Gazali, L., Sztriha, L. *et al.* Mutations in INPP5E, encoding inositol polyphosphate-5-phosphatase E, link phosphatidylinositol signaling to the ciliopathies. *Nat. Genet.* **41**, 1032–1036 (2009).
- 3 Valente, E. M., Logan, C. V., Mougou-Zerelli, S., Lee, J. H., Silhavy, J. L., Brancati, F. *et al.* Mutations in TMEM216 perturb ciliogenesis and cause Joubert, Meckel and related syndromes. *Nat. Genet.* **42**, 619–625 (2010).
- 4 Ferland, R. J., Eyaid, W., Collura, R. V., Tully, L. D., Hill, R. S., Al-Nouri, D. *et al.* Abnormal cerebellar development and axonal decussation due to mutations in AH11 in Joubert syndrome. *Nat. Genet.* **36**, 1008–1013 (2004).
- 5 Parisi, M. A., Bennett, C. L., Eckert, M. L., Dobyms, W. B., Gleeson, J. G., Shaw, D. W. *et al.* The NPHP1 gene deletion associated with juvenile nephronophthisis is present in a subset of individuals with Joubert syndrome. *Am. J. Hum. Genet.* **75**, 82–91 (2004).
- 6 Valente, E. M., Silhavy, J. L., Brancati, F., Barrano, G., Krishnaswami, S. R., Castori, M. *et al.* Mutations in CEP290, which encodes a centrosomal protein, cause pleiotropic forms of Joubert syndrome. *Nat. Genet.* **38**, 623–625 (2006).

- 7 Baala, L., Romano, S., Khaddour, R., Saunier, S., Smith, U. M., Audollent, S. *et al.* The Meckel-Gruber syndrome gene, MKS3, is mutated in Joubert syndrome. *Am. J. Hum. Genet.* **80**, 186–194 (2007).
- 8 Arts, H. H., Doherty, D., van Beersum, S. E., Parisi, M. A., Letteboer, S. J., Gorden, N. T. *et al.* Mutations in the gene encoding the basal body protein RPGRIP1L, a nephrocystin-4 interactor, cause Joubert syndrome. *Nat. Genet.* **39**, 882–888 (2007).
- 9 Cantagrel, V., Silhavy, J. L., Bielas, S. L., Swistun, D., Marsh, S. E., Bertrand, J. Y. *et al.* Mutations in the cilia gene ARL13B lead to the classical form of Joubert syndrome. *Am. J. Hum. Genet.* **83**, 170–179 (2008).
- 10 Gorden, N. T., Arts, H. H., Parisi, M. A., Coene, K. L., Letteboer, S. J., van Beersum, S. E. *et al.* CC2D2A is mutated in Joubert syndrome and interacts with the ciliopathy-associated basal body protein CEP290. *Am. J. Hum. Genet.* **83**, 559–571 (2008).
- 11 Coene, K. L., Roepman, R., Doherty, D., Afroze, B., Kroes, H. Y., Letteboer, S. J. *et al.* OFD1 is mutated in X-linked Joubert syndrome and interacts with LCA5-encoded lebercilin. *Am. J. Hum. Genet.* **85**, 465–481 (2009).
- 12 Davis, E. E., Zhang, Q., Liu, Q., Diplas, B. H., Davey, L. M., Hartley, J. *et al.* TTC21B contributes both causal and modifying alleles across the ciliopathy spectrum. *Nat. Genet.* **43**, 189–196 (2011).
- 13 Dafinger, C., Liebau, M. C., Elsayed, S. M., Hellenbroich, Y., Boltshauser, E., Korenke, G. C. *et al.* Mutations in KIF7 link Joubert syndrome with Sonic Hedgehog signaling and microtubule dynamics. *J. Clin. Invest.* **121**, 2662–2667 (2011).
- 14 Garcia-Gonzalo, F. R., Corbit, K. C., Sirerol-Piquer, M. S., Ramaswami, G., Otto, E. A., Noriega, T. R. *et al.* A transition zone complex regulates mammalian ciliogenesis and ciliary membrane composition. *Nat. Genet.* **43**, 776–784 (2011).
- 15 Huang, L., Szymanska, K., Jensen, V. L., Janecke, A. R., Innes, A. M., Davis, E. E. *et al.* TMEM237 is mutated in individuals with a Joubert syndrome related disorder and expands the role of the TMEM family at the ciliary transition zone. *Am. J. Hum. Genet.* **89**, 713–730 (2011).
- 16 Lee, J. E., Silhavy, J. L., Zaki, M. S., Schroth, J., Bielas, S. L., Marsh, S. E. *et al.* CEP41 is mutated in Joubert syndrome and is required for tubulin glutamylation at the cilium. *Nat. Genet.* **44**, 193–199 (2012).
- 17 Lee, J. H., Silhavy, J. L., Lee, J. E., Al-Gazali, L., Thomas, S., Davis, E. E. *et al.* Evolutionarily assembled cis-regulatory module at a human ciliopathy locus. *Science* **335**, 966–969 (2012).
- 18 Srour, M., Schwartzentruber, J., Hamdan, F. F., Ospina, L. H., Patry, L., Labuda, D. *et al.* Mutations in C50RF42 Cause Joubert Syndrome in the French Canadian Population. *Am. J. Hum. Genet.* **90**, 693–700 (2012).
- 19 Zhang, W., Cui, H. & Wong, L. J. Application of next generation sequencing to molecular diagnosis of inherited diseases. *Top. Curr. Chem.* (e-pub ahead of print 11 May 2012; doi:10.1007/128_2012_325).

Supplementary Information accompanies the paper on Journal of Human Genetics website (<http://www.nature.com/jhg>)



Original Article

Exome sequencing in a family with an X-linked lethal malformation syndrome: clinical consequences of hemizygous truncating *OFD1* mutations in male patients

Tsurusaki Y, Kosho T, Hatasaki K, Narumi Y, Wakui K, Fukushima Y, Doi H, Saitsu H, Miyake N, Matsumoto N. Exome sequencing in a family with an X-linked lethal malformation syndrome: clinical consequences of hemizygous truncating *OFD1* mutations in male patients. Clin Genet 2012. © John Wiley & Sons A/S, 2012

Oral-facial-digital syndrome type 1 (OFD1; OMIM #311200) is an X-linked dominant disorder, caused by heterozygous mutations in the *OFD1* gene and characterized by facial anomalies, abnormalities in oral tissues, digits, brain, and kidney; and male lethality in the first or second trimester pregnancy. We encountered a family with three affected male neonates having an 'unclassified' X-linked lethal congenital malformation syndrome. Exome sequencing of entire transcripts of the whole X chromosome has identified a novel splicing mutation (c.2388+1G > C) in intron 17 of *OFD1*, resulting in a premature stop codon at amino acid position 796. The affected males manifested severe multisystem complications in addition to the cardinal features of OFD1 and the carrier female showed only subtle features of OFD1. The present patients and the previously reported male patients from four families (clinical OFD1; Simpson-Golabi-Behmel syndrome, type 2 with an *OFD1* mutation; Joubert syndrome-10 with *OFD1* mutations) would belong to a single syndrome spectrum caused by truncating OFD1 mutations, presenting with craniofacial features (macrocephaly, depressed or broad nasal bridge, and lip abnormalities), postaxial polydactyly, respiratory insufficiency with recurrent respiratory tract infections in survivors, severe mental or developmental retardation, and brain malformations (hypoplasia or agenesis of corpus callosum and/or cerebellar vermis and posterior fossa abnormalities).

Conflict of interest

The authors have no conflict of interest to declare.

**Y Tsurusaki^{a*}, T Kosho^{b*},
K Hatasaki^c, Y Narumi^b,
K Wakui^b, Y Fukushima^b,
H Doi^a, H Saitsu^a, N Miyake^a
and N Matsumoto^a**

^aDepartment of Human Genetics, Yokohama City Graduate School of Medicine, Yokohama, Japan,

^bDepartment of Medical Genetics, Shinshu University School of Medicine, Matsumoto, Japan, and ^cDepartment of Pediatrics, Toyama Prefectural Central Hospital, Toyama, Japan

*These authors contributed equally to this work.

Key words: exome sequencing – *OFD1* – *OFD1* gene – splicing mutation – X-linked congenital malformation syndrome

Corresponding authors: Tomoki Kosho, MD, Department of Medical Genetics, Shinshu University School of Medicine, 3-1-1 Asahi, Matsumoto, Nagano 390-8621, Japan.

Tel.: +81 263 37 2618;

fax: +81 263 37 2619;

e-mail: ktomoki@shinshu-u.ac.jp

and

Naomichi Matsumoto, MD, PhD, Department of Human Genetics, Yokohama City Graduate School of Medicine, 3-9 Fukuura, Kanazawa-ku, Yokohama 236-0004, Japan.

Tel.: +81 45 787 260;

fax: +81 45 786 5219;

e-mail: naomat@yokohama-cu.ac.jp

Received 14 January 2012, revised and accepted for publication 26 March 2012

Oral-facial-digital syndrome type 1 (OFD1; OMIM #311200), originally described by Papillon-Leage and Psaume (1) and further delineated by Gorlin and Psaume (2), is an X-linked dominant developmental disorder with an estimated prevalence of 1:50,000, caused by mutations in the *OFD1* gene (OMIM #300170) (3–5). The disorder is characterized by facial anomalies and abnormalities in oral tissues, digits, brain and kidney (5). Almost all affected individuals with OFD1 are female, with highly variable expression, possibly resulting from random X inactivation (6). Affected males are generally lost in the first or second trimester of pregnancy (4). To date, only one liveborn male case with clinically definite OFD1 and a normal karyotype has been reported; the patient was born at 34 weeks of gestation and died 21 h after birth due to heart failure (7). In this report, we describe a family with three affected male neonates having an ‘unclassified’ X-linked lethal congenital malformation syndrome. Exome sequencing of entire transcripts of the whole X chromosome has successfully identified a causative splicing mutation in *OFD1*.

Subjects and methods

Clinical report

II-2, a 22-year-old woman, was referred to our clinic for genetic counseling (Fig. 1). Her deceased brother (II-4) had severe multiple congenital abnormalities. She had two sons (III-1 and III-5) with similar congenital abnormalities and a healthy boy (III-3) as well as two miscarriages (III-2, artificial; III-4, spontaneous). During genetic counseling and molecular investigations, she had another healthy boy (III-5). After identification of a heterozygous *OFD1* mutation, she was examined for features of OFD1. Only a few accessory frenulae and irregular teeth with no facial anomalies or tongue abnormalities were observed (Fig. 2a–e). A radiograph of her hands showed no abnormalities (Fig. 2f) and an abdominal ultrasonography detected no cysts in the kidneys, liver, or pancreas (data not shown). I-2, allegedly, had no apparent malformations or complications including renal diseases.

II-4 was born by caesarean section because of placental abruption at 33 weeks of gestation. Pregnancy was complicated by polyhydramnios. Apgar score was 3 at 1 min. His birth weight was 2056 g (+0 SD), length was 45.0 cm (+0.5 SD), and occipitofrontal circumference (OFC) was 34.0 cm (+2.0 SD). He manifested severe respiratory insufficiency and was transferred to a neonatal intensive care unit (NICU). His craniofacial features included a prominent forehead, a large fontanelle (5 × 5 cm), a low posterior hairline, microphthalmia, hypertelorism, short palpebral fissures, depressed nasal bridge, low-set ears, a small cleft lip and a soft cleft palate, narrowing of the tip of the tongue, and a hypoplastic gum (Fig. 2g). Additional physical features included redundant neck skin, postaxial polydactyly of the left hand (Fig. 2h), wide halluces (Fig. 2i), micropenis, and left cryptorchidism.

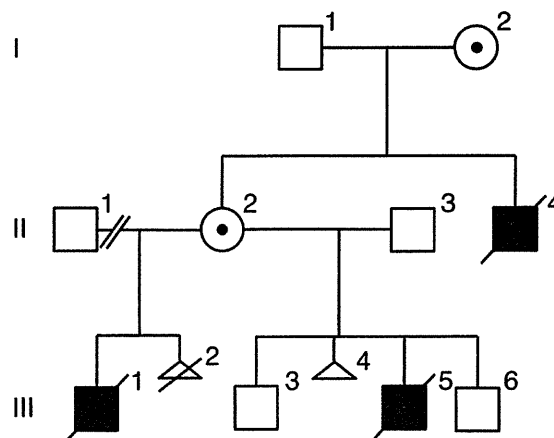


Fig. 1. Familial pedigree.

Ultrasonography revealed hypoplastic gyri, an atrial septal defect, and patent ductus arteriosus. Ophthalmological examination detected microcornea and retinal detachment. Intubation was impossible because of laryngeal anomalies and the patient died 11 h after birth. Additional autopsy findings included partial atelectasis and bilateral hydronephroses.

III-1 was delivered by emergency caesarean section at 39 weeks of gestation. Pregnancy was complicated by polyhydramnios and intrauterine growth retardation, with moderate macrocephaly. His birth weight was 3064 g (+0.1 SD). He was admitted to a NICU because of respiratory insufficiency, and received mechanical ventilation. His craniofacial features included microphthalmia, hypertelorism, short palpebral fissures, epicanthus, low-set ears, and a cleft lip and palate. Additional physical features included bilateral polydactyly of hands (postaxial) and feet (preaxial), and an ectopic urethral opening. Ultrasonography revealed hydrocephalus, agenesis of the corpus callosum and cerebellar vermis, and a complete atrioventricular septal defect. Ophthalmological examination detected persistent pupillary membrane and optic disc coloboma. G-banded chromosomes were normal (46,XY). The patient died at age 14 days due to heart failure.

III-5 was delivered by caesarean section at 32 weeks of gestation. Pregnancy was complicated by polyhydramnios, intrauterine growth retardation, and congenital heart defects. His birth weight was 1704 g (–0.2 SD), length was 40.0 cm (–0.8 SD), and OFC was 33.3 cm (+2.0 SD). He was admitted to a NICU because of respiratory insufficiency, and received mechanical ventilation. His craniofacial features included a prominent forehead, hypertelorism, dysplastic ears, a small cleft lip, and a soft cleft palate (Fig. 2j,k). Ultrasonography revealed hydrocephalus with Dandy-Walker malformation and hypoplastic left heart syndrome. G-banded chromosomes were normal (46,XY). The patient died 1 day after birth. Additional autopsy findings included agenesis of the cerebellar vermis (Fig. 2l), enlargement of the fourth ventricle and aqueduct, anomalous positioning of the esophagus, mild

Exome sequencing in a family with an X-linked lethal malformation syndrome

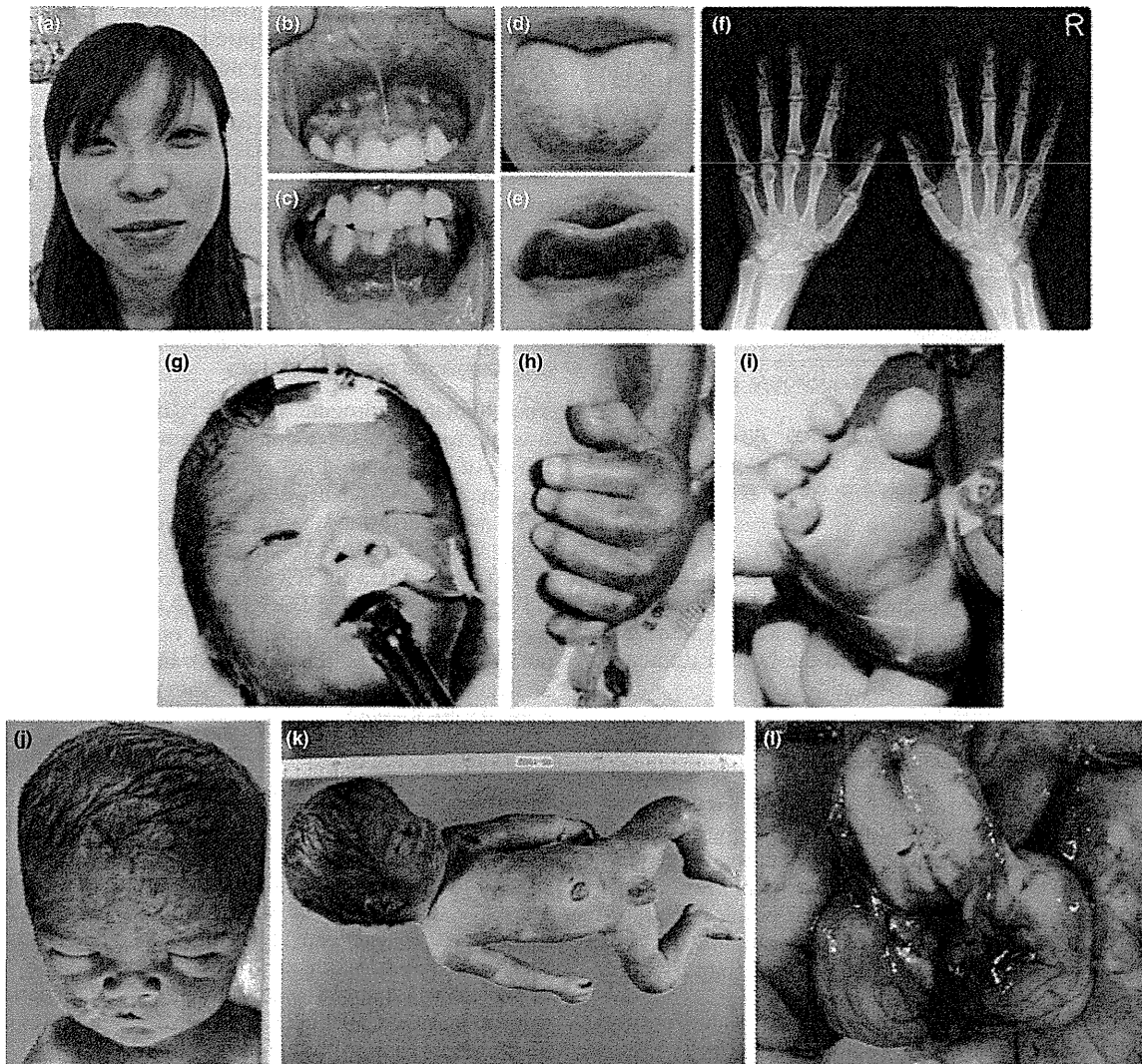


Fig. 2. Clinical photographs of II-2 (a–f), II-4 (g–i), and III-5 (j–l).

pulmonary congestion, and insufficient lobulation of the right lung.

The three affected male neonates, having strikingly similar clinical manifestations (Table 1), are considered to have had a congenital malformation syndrome with X-linked inheritance. Array-CGH analysis using 4200 BAC clones identified no pathologic genomic copy number abnormalities. Direct sequencing of *MID*, performed because of a partial similarity to these neonates' syndrome to X-linked Opitz-G/BBB syndrome (OMIM #300000) (8), revealed no mutation.

Library preparation

Genomic DNA for II-2, II-3, III-3, and III-6 was extracted from peripheral blood using the Gentra PureGene Blood Kit (QIAGEN, Hilden, Germany), and genomic DNA for III-5 was extracted from the preserved dried umbilical cord using the DNeasy Blood

& Tissue Kit (QIAGEN). Three micrograms of high-quality (absorbance at 260 nm/absorbance at 280 nm: 1.8–2.0) genomic DNA from II-2 was fragmented using the Covaris model S2 system (Covaris, Woburn, MA). The target peak size was 150 bp. After the size of sheared DNA was checked using an Agilent 2100 Bioanalyzer (Agilent Technologies, Santa Clara, CA), adapter sequences were ligated to the ends of DNA fragments, and amplified according to the manufacturer's protocol (Agilent Technologies).

Exome capture and next-generation sequencing

Library DNA was hybridized for 24 h at 65°C using the SureSelect Human X Chromosome Demo Kit (Agilent Technologies). Captured DNA was diluted to a concentration of 8 pM and sequenced on a Genome Analyzer IIx (Illumina, San Diego, CA) with 76-bp paired-end reads. We used only one of the eight lanes in the flow

Table 1. Variant priority scheme after exome sequencing^a

	NEXTGENE	II-2	MAQ (SEATTLESEQ)
Total variants called	22,176	—	58,081
Chr X	3441	—	4383
Unknown SNP variants (dbSNP131, 1000 genomes)	910	—	882
Overlap of NEXTGENE and MAQ	—	169	—
NS/SS	—	17	—
Except for variants at segmental duplications	—	15	—

NS, non-synonymous; SNP, single-nucleotide polymorphism; SS, splice site (± 2).

^aMAQ was annotated with SEATTLESEQ ANNOTATION. The annotation includes gene names, dbSNP rs ID, and SNP functions (e.g. missense), protein positions and amino acid changes.

cell for II-2 (Illumina). Image analyses and base calling were performed using sequence control software real-time analysis and OFFLINE BASECALLER software v1.8.0 (Illumina). Reads were aligned to the human reference genome (UCSC hg19, NCBI build 37.1).

Mapping strategy and variant annotation

The quality-controlled (Path Filter) reads were mapped to the human reference genome (UCSC hg19, NCBI build 37.1), using mapping and assembly with quality (MAQ) and NEXTGENE software v2.0 (SoftGenetics, State College, PA). Single-nucleotide polymorphisms in MAQ-passed reads were annotated using the SEATTLESEQ ANNOTATION website (<http://gvs.gs.washington.edu/SeattleSeqAnnotation/>).

Priority scheme and capillary sequencing

Called variants found by each informatics method were filtered in terms of location on chromosome X, unregistered variants (excluding registered dbSNP131 and 1000 Genomes), overlapping variants called in common by NEXTGENE and MAQ, and non-synonymous changes and splice-site mutations (± 2 bp from exon–intron junctions) (Table 1). The variants were confirmed as true positives by Sanger sequencing of polymerase chain reaction (PCR) products amplified using genomic DNA as a template, except for variants within genes at segmental duplications. Sanger sequencing was performed on an ABI3500xl or ABI3100 autosequencer (Life Technologies, Carlsbad, CA). Sequencing data were analyzed using SEQUENCHER software (Gene Codes Corporation, Ann Arbor, MI).

Reverse transcription-PCR

Total RNA was isolated from EBV-transformed lymphoblastoid cell line (EBV-LCL) derived from II-2 and healthy control subjects using the RNeasy Plus Mini

Kit (QIAGEN). Five micrograms of total cellular RNA was used for reverse transcription with the Super Script III First-Strand Synthesis System (Life Technologies). Two microliters of synthesized complementary DNA was used for PCR with the following primers: ex17-F (5'-CTACCATCACCCACTGAGTC-3') and ex19-R (5'-TGAGACATATCCCCGGCAG-3'). Amplified PCR products were electrophoresed in agarose gels, purified from gels using the QIAquick Gel Extraction Kit (QIAGEN), cloned into pCR4-TOPO vector (Life Technologies) and sequenced.

X-chromosome inactivation assay

The human androgen receptor (HUMARA) assay was performed as previously reported (9). Genomic DNA of II-2 was digested at 37°C for 18 h with two methylation-sensitive enzymes, *Hpa*II and *Hha*I. PCR was performed using digested and undigested DNA with HUMARA primers (FAM-labeled ARF: 5'-TCCAGAATCTGTTCCAGAGCGTGC-3'; ARr: 5'-CTCTACGATGGGCTTGGGGAGAAC-3'). DNA fragment analysis was performed on an ABI3130xl autosequencer (Life Technologies). Fragment data were analyzed with GENEMAPPERT SOFTWARE version 4.1 (Life Technologies).

Results

Exome sequencing

Because this disorder was assumed to be an 'X-linked recessive' disorder based on the initial pedigree information, we focused on the X chromosome. Approximately 4.5 Gb of sequence data were generated, 87.3% of which was mapped to the human reference genome (UCSC hg19, NCBI build 37.1). MAQ was able to align 53,242,972 reads to the whole genome.

Two informatics methods identified 17 potential pathogenic changes (15 missense mutations, 1 non-sense mutation, and 1 splice-site mutation) (Table 1). The nonsense mutation was a false positive and all 13 missense mutations were inconsistent with the phenotype (no co-segregation). The mutation c.2388+1G>C was identified at the splice-acceptor site of intron 17 in *OFD1*, heterozygously in II-2, and hemizygotously in III-5, but was absent in II-3, III-3, and III-6 (Fig. 3a) as well as 93 normal female controls (0/186 alleles).

RT-PCR, direct sequencing

To examine the mutational effects of c.2388+1G>C, reverse transcriptase-polymerase chain reaction (RT-PCR) was performed. Only a 239-bp PCR product (wild-type allele) was observed in healthy control individuals (Fig. 3b). By contrast, a longer 1364-bp product was detected in II-2. Sequencing of the 1364-bp product revealed that a 1125-bp sequence of intron 17 was retained, producing a premature stop codon at amino acid position 796 (Fig. 3b). These data indicate

Exome sequencing in a family with an X-linked lethal malformation syndrome

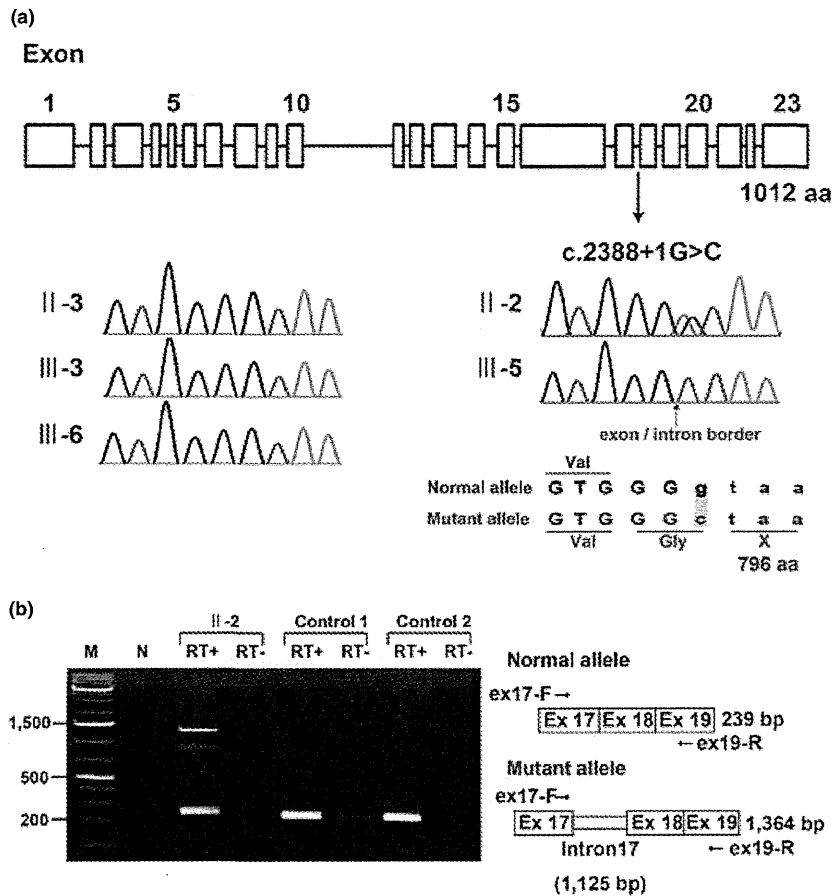


Fig. 3. (a) Gene structure of *OFDI* with the mutation (c.2388+1G>C) (upper). Electropherograms of the family members. Wild-type sequences are seen in II-3, III-3 and III-6. Heterozygous and hemizygous mutations are observed in II-2 and III-5, respectively. (b) Reverse transcriptase-polymerase chain reaction analysis showing both 239-bp and 1364-bp products in II-2, and only 239-bp products in two normal female controls. The 239-bp product is normal and the 1364-bp product is aberrant.

that the c.2388+1G>C mutation in *OFDI* is most likely the causal mutation in this family.

X-chromosome inactivation assay

X-chromosome inactivation patterns was random patterns in II-2 available for this study (ratio > 38:62).

Discussion

Exome sequencing detected a single-base substitution (c.2388+1G>C) in *OFDI*, resulting in an error in splicing of intron 17 and a premature stop codon at amino acid position 796, in an affected male (III-5) and a carrier female (II-2) in this family with an 'unclassified' X-linked lethal congenital malformation syndrome. II-4 and III-1, who had strikingly similar clinical manifestations to III-5, are likely to have had the same *OFDI* mutation as III-5, although their DNA was not available. Through reassessment of clinical features of the family, the three affected males shared facial, oral, and digital malformations characteristic of OFD1 (4). Additionally, they exhibited more severe

complications in various systems including congenital heart defects, genitourinary malformations, and ophthalmological abnormalities. II-2 was also found to have subtle features of OFD1 (accessory frenulae and irregular teeth). Thus, we have concluded that the 'unclassified' X-linked lethal congenital malformation syndrome in this family was clinically compatible with OFD1.

An *OFDI* mutation (c.2123_2126dupAAGA in exon 16, p.Asn711Lysfs*3) was also detected in a family with an X-linked recessive mental retardation syndrome (10). Nine affected males had macrocephaly and severe mental or developmental retardation, and suffered from recurrent respiratory tract infections leading to early death in eight. Only an 11-year-old boy survived with severe mental retardation (IQ 20), obesity, and brachydactyly. His younger brother had postaxial polydactyly. No cognitive, oral, facial, digital, or renal abnormalities were detected in heterozygous carrier females in that family. The patients were later classified into an infantile lethal variant of Simpson-Golabi-Behmel syndrome (type 2) (SGBS2, OMIM #300209), which had consisted of only one family,

genetically mapped to Xp22, including four maternally related affected males with hydrops at birth, craniofacial anomalies (macrocephaly, low-set posteriorly angulated ears, hypertelorism, short and broad nose with anteverted nares, large mouth with thin upper vermilion border, prominent philtrum, high-arched or cleft palate, and short neck), redundant skin, hypoplastic nails, skeletal defects involving upper and lower limbs, gastrointestinal and genitourinary anomalies, hypotonia and neurological impairment, and early death within the first 8 weeks (11, 12). Other *OFDI* mutations were detected in two families with Joubert syndrome-10 (JBTS10, OMIM #213300) (13). A mutation (c.2844_2850delAGACAAA in exon 21, p.Lys948Asnfs*9) in a family with eight affected males caused severe mental or developmental retardation and recurrent infections in all; postaxial polydactyly in five, retinitis pigmentosa in three, and a molar tooth sign on brain magnetic resonance imaging (MRI) in two. No heterozygous carrier females had any symptoms similar to those in the affected males. Another mutation (c.2767delG in exon 21, p.Glu923Lysfs*4) was found *de novo* in a 12-year-old male patient with severe mental retardation, macrocephaly, obesity, postaxial polydactyly, and a molar tooth sign on brain MRI (13).

To discuss whether these male patients with hemizygous truncating *OFDI* mutations would have different conditions (OFD1, SGBS2, or JBTS10) or belong to the same syndrome spectrum, we have created a comprehensive list of clinical manifestations in all of them (Table 2) (7, 10, 13). Macrocephaly, polydactyly (postaxial), respiratory insufficiency with recurrent respiratory tract infections in survivors, and severe mental or developmental retardation were shared by all the families (7, 10, 13). Nasal bridge features (depressed or broad) and lip abnormalities (cleft lip, pseudocleft lip, full lips, and prominent philtrum) were shared by the families with OFD1 and JBTS10 (7, 13). Brain malformations including hypoplasia or agenesis of corpus callosum, hypoplasia or agenesis cerebellar vermis as well as posterior fossa abnormalities (large, occipital encephalocele) were also shared by the families with OFD1 and JBTS10 (7, 13). III-5 in the present family was described to have Dandy-Walker malformation on brain ultrasonography. Three patients with JBTS10 were described to have a molar tooth sign on brain MRI, which is the characteristic neuroradiological hallmark of Joubert syndrome (13). Dandy-Walker malformation, typically consisting of agenesis or hypoplasia of cerebellar vermis, a cystic dilatation of the fourth ventricle, and an enlarged posterior fossa with a high position of the tentorium, is usually distinguishable from Joubert syndrome, characterized anatomically by agenesis or hypoplasia of cerebellar vermis and enlargement of the superior cerebellar peduncles and deep interpeduncular fossa resulting from a lack of normal decussation of superior cerebellar peduncular fiber tracts, leading to the characteristic 'molar tooth' appearance on transverse computed tomography and MRI of the mid-brain (14); and clinically by hypotonia, developmental

retardation, abnormal respiratory patterns, and oculomotor apraxia (15). However, Joubert syndrome could be present in association with Dandy-Walker malformation (15); and in such a case, Dandy-Walker malformation was reported to have initially masked the molar tooth sign because of a cystic dilatation of the fourth ventricle (16). Some authors state that the presence of the molar tooth sign does not, in itself, allow a diagnosis, Joubert syndrome, to be made; but that clinical evidence of the syndrome including hypotonia and developmental retardation accompanied by either abnormal breathing or abnormal eye movements should be present (14, 17). Typical respiratory abnormalities in Joubert syndrome, represented by short alternate episodes of apnea and hyperpnea or episodic hyperpnea alone (18), were not described in the patients with JBTS10, with only one presenting with stridor and intermittent cyanosis soon after birth (13). Abnormal eye movements including oculomotor apraxia were not mentioned in those with JBTS10 (13). In view of these evidences, it is reasonable to consider that the male patients with *OFDI* mutations, identified to date, would belong to a clinical continuum with wide intra- and inter-familial phenotypic variations of a single disorder.

A review by Macca and Franco (4) summarized all reported mutations in OFD1 patients. In total, 99 different mutations (7 genomic deletions and 92 point mutations) were identified, including 67 frameshift mutations (58%), 14 missense mutations (12%), 14 splice-site mutations (12%), 13 nonsense mutations (11%), and an in-frame deletion. Point mutations occur only in the first 17 exons (*OFDI* consists of 23 exons). A significant genotype-phenotype correlation between high-arched/cleft palate and missense and splice-site mutations has been identified (19). In addition, cystic kidney is more frequently associated with mutations in exons 9 and 12 (19). Quantitative PCR analysis of *OFDI* mRNA levels in EBV-LCLs from two families with JBTS10 showed that 30% and 58% of *OFDI* expression remained, suggesting that the mutant mRNA would be subject to nonsense-mediated decay and that the phenotypic variability observed for *OFDI* mutations would be caused by changes in activity of remaining truncated OFD1 protein (13). To date, premature stop codons at 713 in exon 16 (19), 796 in exon 17 (this report), 926 in exon 21 (13), and 956 in exon 21 (13) are associated with survival in males with hemizygous truncating *OFDI* mutations and no or subtle clinical manifestations in females with heterozygous *OFDI* mutations. Heterozygous truncating *OFDI* mutations preserving normal exons 1-16 have been reported in only two families with typical female OFD1 patients: a single-base deletion (c.2349delC in exon 17, p.Ileu784Serfs*85) (20) and a deletion of complete exon 17 (21). Mutations producing longer truncated protein (~ exon 17) might cause a milder form of the disorder that could not be detected in typical female OFD1 patients, but could be detected in male patients with multiple congenital anomalies and probable lethality in childhood.

Table 2. Clinical features of male patients with *OFD1* mutations

Patient	Family 1 (present family)			Family 2 ^b	Family 3 ^c			Family 4 ^d (W07-713)			Family 5 ^d (UW87)	Carrier	
	II-4	III-1	III-5	1	IV-1	IV-3	IV-11	6 Patients	III-9	IV-10	6 Patients		19 Females
Age	0d/D	14d/D	1d/D		11 y	18 m/D	3 y/D	D	34 y	3.5 y	D (3)		
Birth weight (g) (gestational age)	2056 (33)	3064 (39)	1704 (32)		3850 (40)	4120 (38)	1915 (35)			3050 (Te)		4090 (41)	
Macrocephaly (>1.5 SD)	+		+		+	+	+	Some				+	
Obesity					+				-	-	-	+	
Craniofacial (87.3% ^a)									-	-	-		
Facial anomalies (69.1% ^a)													
Prominent forehead	+		+										
Redundant neck skin	+											+	
Hypertelorism	+	+	+	+									
Epicanthus		+											
Short palpebral fissures	+	+											
Nasal bridge features	Dep		Dep						Br	Br		Dep	
Low-set ears	+	+			+				+	+			
Lip abnormalities (32.6% ^a)	PCL	CL	PCL	PCL					FL, PP	FL, PP		PCL	PCL (1)
Oral													
Palatal abnormalities (49.6% ^a)	CSP	CP	CSP	CSP	HP								
Accessory frenulae (63.7% ^a)													+
Tongue abnormalities (84.1% ^a)	Nar											MG	Lob (3)
Teeth abnormalities (43.3% ^a)													Ir (1)
Skeletal													
Short fingers/brachydactyly					+		+			-	-	+	
Postaxial polydactyly (3.7% ^a)	LtH	BiH		BiHRtBLT		RtH				BiHF	BiHF (4)	BiHLtF	
Preaxial polydactyly (19.3% ^a)	BiBrHx	BIF		BIBHx	BiBrT								
Respiratory													
Laryngeal anomalies	+												
Respiratory insufficiency	+	+				+				+			
Recurrent infections					+	+	+	+	+	+	+	+	+
Cardiovascular													
Congenital heart defects	ASD, PDA	AVSD	HLHS	AVSD									
Genitourinary													
Cystic kidney	-		-		-	-			-	-	-	-	
Urinary tract abnormalities	HU	EUO											
Genital abnormalities	MP, C												
Gastrointestinal													
Esophageal abnormalities			+										
Ophthalmological													
Microphthalmia/microcornea	+												
Persistent papillary membrane		+											

Exome sequencing in a family with an X-linked lethal malformation syndrome

Table 2. Continued

Patient	Family 1 (present family)			Family 2 ^b	Family 3 ^c				Family 4 ^d (W07-713)			Family 5 ^d (UW87)	Carrier 19 Females
	II-4	III-1	III-5	1	IV-1	IV-3	IV-11	6 Patients	III-9	IV-10	6 Patients		
Optic disc coloboma		+											
Optic nerve atrophy													+
Retinal detachment	+												
Retinitis pigmentosa									+	+	+(1)		-
Central nervous system (48.4% ^a)													
Hydrocephalus		+	+	+	-	-	+						
Gyrus abnormalities	Hp			PM	-	-	-						
Corpus callosum abnormalities		Ag		Ag	-	-	-						Hp
Cerebellar vermis abnormalities		Ag	Ag		-	-	-		Hp	Hp			
Thick superior cerebellar peduncles					-	-	-		+	+			
Molar tooth sign					-	-	-		+	+			+
Dandy-Walker malformation			+		-	-	-						
Posterior fossa abnormalities				L	-	-	-			L			EC
Developmental/mental retardation					S	S	+	S	S	S	+(All)		S

+, present; -, absent; blank, data not available; Ag, agenesis; ASD, atrial septal defect; AVSD, atrioventricular septal defect; BHx, bifid halluces; Bi, bilateral; BLT, bifid little toe; Br, broad; C, cryptorchidism; CL, cleft lip; CP, cleft palate; CSP, cleft soft palate; d, days; D, death; Dep, depressed; EC, encephalocele; EUO, ectopic urethral opening; F, foot/feet; FL, full lips; H, hand(s); HF, hands and feet; HLHS, hypoplastic left heart; Hp, hypoplasia; HP, high palate; HU, hydroureter; Hx, halluces; Ir, irregular; L, large; Lob, lobulated; Lt, left; m, months; MG, midline groove; MP, micropenis; Nar, narrowing of the tip of the tongue; PCL, pseudocleft of the upper lip; PDA, patent ductus arteriosus; PM, polymicrogyria; PP, prominent philtrum; Rt, right; S, severe; Te, term; T, thumbs; y, years.

^aFrom Macca and Franco (4).

^bFrom Goodship et al. (7).

^cFrom Budny et al. (10).

^dFrom Coene et al. (13).

Exome sequencing in a family with an X-linked lethal malformation syndrome

High-throughput, next-generation sequencing (NGS) has had a tremendous impact on human genetic research (22). Moreover, techniques enabling enrichment of selected regions enable us to use NGS efficiently and to identify the causative genes for a reasonable number of genetic disorders as well as susceptibility genes for complex diseases and health-related traits (23). In particular, X-linked disorders are good candidates for exome sequencing. We recently identified a nonsense mutation in *MCT8* causing X-linked leukoencephalopathy in a family from only two affected male samples (24). We have also identified two possible but inconclusive missense variants (*LICAM* and *TMEM187*) in a family with an atypical X-linked leukodystrophy from only two affected male samples (25). In this study, exome sequencing accompanied by appropriate bioinformatics techniques and a co-segregation evaluation successfully revealed a disease-causing mutation in *OFD1*, which could not have been assumed to be a candidate based on the clinical manifestations of the affected male patients. Unbiased rapid screening through these technologies is a powerful method for the detection of mutations in unexpected causative genes in undiagnosed patients with multiple congenital malformations.

In conclusion, we have identified a causative splicing mutation in *OFD1*, through exome sequencing, in a family with three males having an 'unclassified' X-linked lethal congenital malformation syndrome. The affected males manifested severe multisystem complications in addition to the cardinal features of *OFD1* and the carrier female showed only subtle features of *OFD1*. The present patients, as well as the previously reported male patients from four families (one with clinical *OFD1*; one with *SGBS2* and an *OFD1* mutation; two with *JBTS10* and *OFD1* mutations), would belong to a single syndrome spectrum caused by truncating *OFD1* mutations, presenting with craniofacial features (macrocephaly, depressed or broad nasal bridge, and lip abnormalities), postaxial polydactyly, respiratory insufficiency with recurrent respiratory tract infections in survivors, severe mental or developmental retardation, and brain malformations (hypoplasia or agenesis of corpus callosum and/or cerebellar vermis and posterior fossa abnormalities).

Acknowledgements

The authors are grateful to the family for their participation in this study. The authors are also thankful to Prof Germana Meroni (Cluster in Biomedicine, Trieste) for mutation analysis of *MIDI1*, Dr Takeshi Futatani (Department of Pediatrics, Toyama Prefectural Central Hospital, Toyama, Japan), Dr Masahiko Kawabata (Department of Internal Medicine, Toyama Prefectural Central Hospital, Toyama, Japan), and Dr Akio Uchiyama (Department of Pathology, Toyama Prefectural Central Hospital, Toyama, Japan) for collecting clinical information; Dr Gen Nishimura (Department of Radiology, Tokyo Metropolitan Children's Medical Center) for helping radiological assessment; and Miss Junko Kunimi (Department of Medical Genetics, Shinshu University School of Medicine, Matsumoto, Japan) and Dr Shin-ya Nishio (Department of Otolaryngology, Shinshu University School of Medicine, Matsumoto,

Japan) for their technical assistance. This work was supported by research grants from the Ministry of Health, Labour and Welfare (T. K., Y. F., H. S., N. Mi., and N. Ma.), the Japan Science and Technology Agency (N. Ma.), the Strategic Research Program for Brain Sciences (N. Ma.) and a Grant-in-Aid for Scientific Research on Innovative Areas (Foundation of Synapse and Neuro-circuit Pathology) from the Ministry of Education, Culture, Sports, Science and Technology of Japan (N. Ma.), a Grant-in-Aid for Scientific Research from Japan Society for the Promotion of Science (N. Ma.), a Grant-in-Aid for Young Scientist from Japan Society for the Promotion of Science (H. S. and N. Mi.) and a grant from the Takeda Science Foundation (N. Mi. and N. Ma.). This work was performed at the Advanced Medical Research Center, Yokohama City University, Japan.

Y. T., H. D., H. S., and N. Mi. performed the genetic analysis; T. K., K. H., Y. N., K. W., and Y. F. evaluated clinical aspects of the family, recruited samples, and prepared them for the analysis. Y. T., T. K. and N. Ma. wrote the manuscript.

Ethics approval

The work was approved by the Yokohama City University (Faculty of Medicine) and the Shinshu University (School of Medicine). Patient consent was obtained.

References

1. Papillon-Leage M, Psaume J. Une malformation hereditaire de la muqueuse buccale: brides et freins anomaux. *Rev Stomatol* 1954; 55: 209–227.
2. Gorlin RJ, Psaume J. Orofaciodigital dysostosis: a new syndrome. A study of 22 cases. *J Pediatr* 1962; 61: 520–530.
3. Ferrante MI, Giorgio G, Feather SA et al. Identification of the gene for oral-facial-digital type I syndrome. *Am J Hum Genet* 2001; 68: 569–576.
4. Macca M, Franco B. The molecular basis of oral-facial-digital syndrome, type I. *Am J Med Genet C* 2009; 151C: 318–325.
5. Toriello HV, Franco B. Oral-facial-digital syndrome type I. In: Pagon RA, Bird TD, Dolan CR, Stephens K, Adam MP, eds. *GeneReviews at genetests: Medical Genetics Information Resource* (database online). Seattle, WA: Copyright, University of Washington, 1993–2011, from <http://www.genetests.org>. Accessed on July 23, 2011.
6. Morleo M, Franco B. Dosage compensation of the mammalian X-chromosome influences the phenotypic variability of X-linked dominant male-lethal disorders. *J Med Genet* 2008; 45: 401–408.
7. Goodship J, Platt J, Smith R, Burn J. A male with type I orofaciadigital syndrome. *J Med Genet* 1991; 28: 691–694.
8. Fontanella B, Russolillo G, Meroni G. *MIDI1* mutations in patients with X-linked Opitz G/BBB syndrome. *Hum Mutat* 2008; 29: 584–594.
9. Nishimura-Tadaki A, Wada T, Bano G et al. Breakpoint determination of X;autosome balanced translocations in four patients with premature ovarian failure. *J Hum Genet* 2011; 56: 156–160.
10. Budny B, Chen W, Omran H et al. A novel X-linked recessive mental retardation syndrome comprising macrocephaly and ciliary dysfunction is allelic to oral-facial-digital type I syndrome. *Hum Genet* 2006; 120: 171–178.
11. Terespolsky D, Farrell SA, Siegel-Bartelt J, Weksberg R. Infantile lethal variant of Simpson-Golabi-Behmel syndrome associated with hydrops fetalis. *Am J Med Genet* 1995; 59: 329–333.
12. Brzustowicz LM, Farrell S, Khan MB, Weksberg R. Mapping of a new *SGBS* locus to chromosome Xp22 in a family with a severe form of Simpson-Golabi-Behmel syndrome. *Am J Hum Genet* 1999; 65: 779–783.
13. Coene KL, Roepman R, Doherty D et al. *OFD1* is mutated in X-linked Joubert syndrome and interacts with *LCA5*-encoded lebercilin. *Am J Hum Genet* 2009; 85: 465–481.
14. McGraw P. The molar tooth sign. *Radiology* 2002; 229: 671–672.
15. Chance PF, Cavalier L, Satran D, Pellegrino JE, Koenig M, Dobyns WB. Clinical nosologic and genetic aspects of Joubert and related syndromes. *J Child Neurol* 1999; 14: 660–666.

Tsurusaki et al.

16. Sartori S, Ludwig K, Fortuna M et al. Dandy-Walker malformation masking the molar tooth sign: an illustrative case with magnetic resonance imaging follow-up. *J Child Neurol* 2010; 25: 1419–1422.
17. Barkovich AJ. Anomalies with cerebellar dysgenesis: vermian dysgenesis. In: Barkovich AJ, ed. *Pediatric neuroimaging*, 4th edn. Lippincott Williams & Wilkins, Philadelphia 2005: 391–396.
18. Brancati F, Dallapiccola B, Valente EM. Joubert syndrome and related disorders. *Orphanet J Rare Dis* 2010; 5: 20.
19. Prattichizzo C, Macca M, Novelli V et al. Mutational spectrum of the oral-facial-digital type I syndrome: a study on a large collection of patients. *Hum Mutat* 2008; 29: 1237–1246.
20. Thauvin-Robinet C, Cossée M, Cormier-Daire V et al. Clinical, molecular, and genotype-phenotype correlation studies from 25 cases of oral-facial-digital syndrome type 1: a French and Belgian collaborative study. *J Med Genet* 2006; 43: 54–61.
21. Thauvin-Robinet C, Franco B, Saugier-Veber P et al. Genomic deletions of *OFDI* account for 23% of oral-facial-digital type 1 syndrome after negative DNA sequencing. *Hum Mutat* 2008; 30: E320–E329.
22. Shendure J, Ji H. Next-generation DNA sequencing. *Nat Biotechnol* 2008; 26: 1135–1145.
23. Bamshad MJ, Ng SB, Bigham AW et al. Exome sequencing as a tool for Mendelian disease gene discovery. *Nat Rev Genet* 2011; 12: 745–755.
24. Tsurusaki Y, Osaka H, Hamanoue H et al. Rapid detection of a mutation causing X-linked leukodystrophy by exome sequencing. *J Med Genet* 2011; 48: 606–609.
25. Tsurusaki Y, Okamoto N, Suzuki Y et al. Exome sequencing of two patients in a family with atypical X-linked leukodystrophy. *Clin Genet* 2011; 80: 161–166.

Mitochondrial Complex III Deficiency Caused by a Homozygous *UQCRC2* Mutation Presenting with Neonatal-Onset Recurrent Metabolic Decompensation

Noriko Miyake,^{1*†} Shoji Yano,^{2†} Chika Sakai,³ Hideyuki Hatakeyama,³ Yuichi Matsushima,³ Masaaki Shiina,⁴ Yoriko Watanabe,⁵ James Bartley,⁶ Jose E. Abdenur,⁷ Raymond Y. Wang,⁷ Richard Chang,⁷ Yoshinori Tsurusaki,¹ Hiroshi Doi,¹ Mitsuko Nakashima,¹ Hiroto Saito,¹ Kazuhiro Ogata,⁴ Yu-ichi Goto,³ and Naomichi Matsumoto^{1*}

¹Department of Human Genetics, Yokohama City University Graduate School of Medicine, Yokohama, Japan; ²Genetics Division, Department of Pediatrics, LAC + USC Medical Center, Keck School of Medicine, University of Southern California, Los Angeles, California; ³Department of Mental Retardation and Birth Defect Research, National Institute of Neuroscience, NCNP, Kodaira, Tokyo, Japan; ⁴Department of Biochemistry, Yokohama City University Graduate School of Medicine, Yokohama, Japan; ⁵Department of Pediatrics and Child Health, Kurume University School of Medicine, Kurume, Japan; ⁶Division of Medical Genetics, Department of Pediatrics, Children's Hospital Los Angeles, Los Angeles, California; ⁷Division of Metabolic Disorders, CHOC Children's, Orange, California

Communicated by Daniel Nebert

Received 26 June 2012; accepted revised manuscript 7 November 2012.

Published online 19 December 2012 in Wiley Online Library (www.wiley.com/humanmutation). DOI: 10.1002/humu.22257

ABSTRACT: Mitochondrial complex III (CIII) deficiency is a relatively rare disease with high clinical and genetic heterogeneity. CIII comprises 11 subunits encoded by one mitochondrial and 10 nuclear genes. Abnormalities of the nuclear genes such as *BCS1L* and *TTC19* encoding mitochondrial assembly factors are well known, but an explanation of the majority of CIII deficiency remains elusive. Here, we report three patients from a consanguineous Mexican family presenting with neonatal onset of hypoglycemia, lactic acidosis, ketosis, and hyperammonemia. We found a homozygous missense mutation in *UQCRC2* that encodes mitochondrial ubiquinol-cytochrome *c* reductase core protein II by whole-exome sequencing combined with linkage analysis. On the basis of structural modeling, the mutation (p.Arg183Trp) was predicted to destabilize the hydrophobic core at the subunit interface of the core protein II homodimer. In vitro studies using fibroblasts from the index patient clearly indicated CIII deficiency, as well as impaired assembly of the supercomplex formed from complexes I, III, and IV. This is the

first described human disease caused by a core protein abnormality in mitochondrial CIII.

Hum Mutat 00:1–10, 2012. © 2012 Wiley Periodicals, Inc.

KEY WORDS: mitochondrial complex III (CIII); *UQCRC2*; whole exome sequence; supercomplex

Introduction

The mitochondrial respiratory chain generates energy as ATP by means of the electron-transport chain and the oxidative-phosphorylation system. The mitochondrial respiratory chain, located in the inner mitochondrial membrane, is composed of five multimeric protein complexes: I, II, III, IV, and V. Among them, the complex III (CIII) (bc1 complex or ubiquinol-cytochrome *c* reductase; EC1.10.2.2) monomer is composed of 11 proteins [Iwata et al., 1998]. One protein is encoded by mitochondrial DNA (*MTCYB*) and the other 10 are encoded by nuclear DNA. The latter are categorized into three groups: (1) core proteins (encoded by *UQCRC1* and *UQCRC2*), (2) respiratory proteins (*CYC1* and *UQCRFS1*), and (3) low-molecular-weight proteins (*UQCRH*, *UQCRB*, *UQCRQ*, *UCRC*, *UQCR11*, and *UQCRFS1*). In its native state, the CIII monomer is quickly converted into a catalytically active homodimer that is incorporated into a supercomplex (respirasome) with complexes I and IV, and this supercomplex functions as a single enzyme [Schagger and Pfeiffer, 2000].

Mitochondrial CIII enzyme deficiency (CIII deficiency; MIM# 124000) is a relatively rare disease with clinical and genetic heterogeneity. Until now, mutations in four genes have been known to cause autosomal recessive CIII deficiencies: *UQCRB* (NM_006294), *UQCRQ* (NM_014402), *BCS1L* (NM_004328), and *TTC19* (NM_017775). *UQCRB* and *UQCRQ* encode components of CIII itself, whereas *BCS1L* and *TTC19* produce mitochondrial assembly factors. Although recessive *BCS1L* mutations are the most frequent cause of CIII deficiency, the majority of the genetic causes of CIII deficiency remain unknown [Benit et al., 2009; de Lonlay et al.,

Additional Supporting Information may be found in the online version of this article.

†These authors contributed equally to this work.

*Correspondence to: Noriko Miyake, Department of Human Genetics, Yokohama City University Graduate School of Medicine, 3-9 Fukuura, Kanazawa-ku, Yokohama 236-0004, Japan. E-mail: noriko.miyake@yokohama-cu.ac.jp; or Naomichi Matsumoto, Department of Human Genetics, Yokohama City University Graduate School of Medicine, 3-9 Fukuura, Kanazawa-ku, Yokohama 236-0004, Japan. E-mail: naomat@yokohama-cu.ac.jp

Contract grant sponsors: Ministry of Health, Labor, and Welfare; the Japan Science and Technology Agency; the Strategic Research Program for Brain Sciences; Ministry of Education, Culture, Sports, Science, and Technology of Japan; the Japan Society for the Promotion of Science; 2011 Strategic Research Promotion of Yokohama City University; the Japan Epilepsy Research Foundation; and the Takeda Science Foundation.

2001; DiMauro and Schon, 2003; Fernandez-Vizarrá et al., 2007; Hinson et al., 2007; Visapaa et al., 2002]. Interestingly, *BCS1L* mutations cause variable clinical presentations: Bjornstad syndrome (MIM# 262000), which is characterized by sensorineural hearing loss and pili torti [Hinson et al., 2007]; GRACILE syndrome (MIM# 603358), which presents with fetal growth retardation, aminoaciduria, cholestasis, iron overload, lactic acidosis, and early death [Visapaa et al., 2002]; and Leigh syndrome (MIM# 256000) [de Lonlay et al., 2001]. A homozygous mutation of *TTC19* causes a progressive neurodegenerative disorder [Ghezzi et al., 2011]. A homozygous 4-bp deletion of *UQCRB* causes hypoglycemia and lactic acidosis [Haut et al., 2003] and a homozygous missense mutation of *UQCRCQ* results in severe psychomotor retardation, extrapyramidal signs, and dementia [Barel et al., 2008].

Here, we describe the first human mutation of *UQCRC2* encoding core protein 2 of CIII, utilizing linkage analysis and whole-exome sequencing.

Materials and Methods

DNA Preparation

DNAs from family members and fibroblasts from patients were collected after obtaining informed consent. DNA was extracted from blood leukocytes using a QIAamp DNA Blood Midi Kit (Qiagen, Hilden, Germany) or QuickGene-610L (Fujifilm, Tokyo, Japan), according to the manufacturers' instructions. DNAs from 80 Mexican control subjects were purchased from the Coriell Institute for Medical Research (Camden, New Jersey). The experimental protocols were approved by the institutional review board of Yokohama City University.

Linkage Analysis

SNP typing was performed using an Affymetrix Human Mapping SNP 10K Xba I 142 2.0 array (Affymetrix, Santa Clara, California), according to the manufacturer's instructions. A multipoint linkage analysis was performed using Allegro version 2.0 [Gudbjartsson et al., 2005]. An autosomal recessive mode of inheritance with complete penetrance and a disease allele frequency of 0.005 was used.

Exome Sequence

Briefly, 3 μ g of genomic DNA was sheared and captured using a NimbleGen SeqCap EZ Exome Library SR (Roche NimbleGen, Inc., Madison, New Jersey), according to the manufacturer's instructions. The captured sample was sequenced on a GAIIX instrument (Illumina, Inc., San Diego, California) using 76-bp paired-end reads. Image analysis and base calling were performed by sequence-control software real-time analysis (Illumina, Inc.) and CASAVA software v1.7 (Illumina, Inc.). The quality-controlled (path-filtered) reads were mapped to human genome reference hg19 with Mapping and Assembly with Qualities (MAQ; <http://maq.sourceforge.net/>) and NextGENe software v2.00 (SoftGenetics, State College, Pennsylvania). The variants from MAQ were annotated by SeattleSeq annotation 131 (<http://snp.gs.washington.edu/SeattleSeqAnnotation131>). The priority scheme of the variants was described previously [Tsurusaki et al., 2011]. The nucleotide numbering of the variants reflects the cDNA numbering, with +1 corresponding to the A of the ATG translation initiation codon in the reference sequence, accord-

ing to journal guidelines (www.hgvs.org/mutnomen). The initiation codon is codon 1.

Expression Vector Preparation

For construction of a mammalian expression vector, full-length *UQCRC2* (NM_003366.2) was amplified from a cDNA library from a multiple-tissue cDNA (MTC) panel (Clontech, Mountain View, California) using KOD-plus DNA polymerase (Toyobo, Osaka, Japan). The PCR product was cloned into the entry vector (pDONRTM221) of the gateway system (Invitrogen, Carlsbad, California). Each of the two missense mutations was independently introduced into the entry clone using a QuickChange II XL site-directed mutagenesis kit (Stratagene, La Jolla, California). Each insert was cloned into pcDNA-DEST40 (C-terminal V5 and 6xHis tag) by LR recombination. All the clones were verified by direct sequencing. In addition, full-length *UQCRC2* (wild type, mutant, or SNP [rs4850: c.548G>A, p.Arg183Gln]) and AcGFP constructs were cloned into multiple cloning sites A and B of the pIRES vector (Clontech).

Intracellular Localization

Each mammalian expression construct (200 ng) was transfected into COS-1 cells using FuGENE6 (Roche Diagnostics, Indianapolis, Indiana). After 24 hr of transfection, MitoTracker Red CMXRos (Invitrogen) was added and incubated for 30 min. The cells were then fixed with 4% paraformaldehyde for 20 min at room temperature. After permeabilization with 0.1% Triton/1 \times PBS for 10 min, C-terminally V5-6xHis-tagged *UQCRC2* protein was stained with a mouse anti-V5 antibody (1:1,000) (Invitrogen) and an Alexa Fluor 488-conjugated goat antimouse IgG secondary antibody (1:1,000) (Molecular Probes, Carlsbad, California). Confocal images were taken with a FLUOVIEW FV1000-D microscope (Olympus, Tokyo, Japan).

Mitochondrial Enzyme Activity Assay

Mitochondrial enzyme activities were measured using a previously reported method [Trounce et al., 1996], with slight modifications. The complex I activity is indicated as the rotenone-sensitive NADH-CoQ1 reductase activity. In control assays, the activity was decreased to 20% by rotenone.

Western Blotting

Mitochondrial enzyme activity and supercomplex formation were analyzed by western blotting. The enzyme activities of the mitochondrial respiratory chain complexes were measured using mitochondrial fractions prepared from primary fibroblasts derived from patient 1 ($n = 3$) and control subjects ($n = 10$). Each measurement was basically performed in triplicate (if the available materials allowed). The values were normalized to complex II or citrate synthase. Immunoblot detection of each respiratory chain complex was performed using mitochondria solubilized with 0.5% *n*-dodecyl- β -D-maltoside (DDM). The same amount of pooled mitochondrial protein from control subjects ($n = 10$) was used as the control. The primary antibodies used were as follows: 2 μ g/ml anti-NDUFA9 (complex I; Invitrogen), 0.02 μ g/ml anti-SDHA (complex II; Invitrogen), 2 μ g/ml anti-UQCRC1 (CIII; Abcam, Cambridge, Massachusetts), 0.2 μ g/ml anti-MTCO1 (complex IV; Invitrogen), and

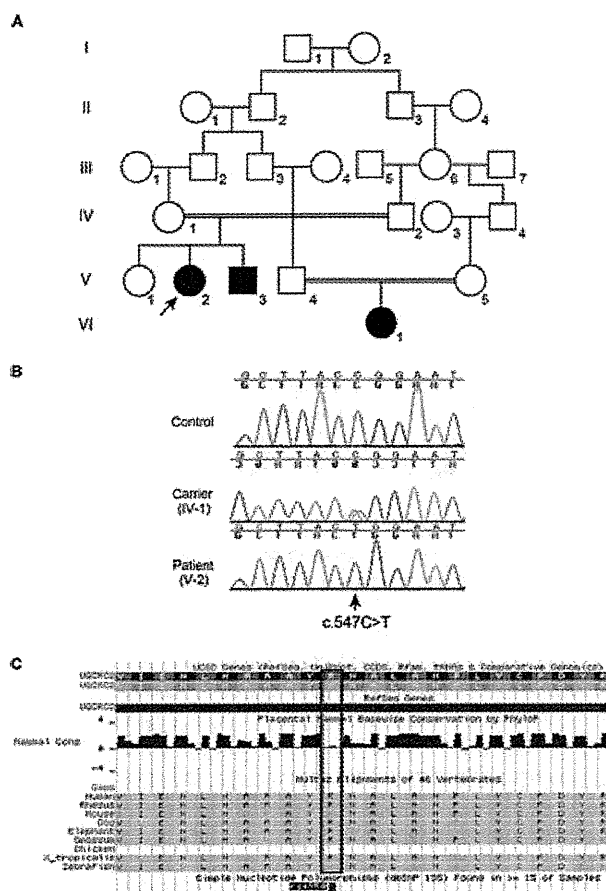


Figure 1. Identification of a *UQCRC2* mutation in a consanguineous Mexican family. **A:** Pedigree of the reported family. The arrow indicates the proband. **B:** Electropherogram of the c.547C>T *UQCRC2* mutation. All three patients (1, 2, and 3) showed a homozygous change, whereas the parents and an unaffected sibling of patients 1 and 2 were heterozygous carriers. The arrow indicates c.547C>T. **C:** Evolutionary conservation of p.Arg183 in *UQCRC2* outlined in red. rs4850 (chr 16: 21976762, G>A, p.Arg183Gln) is a common SNP based on the dbSNP135 database.

2 $\mu\text{g/ml}$ anti-ATP5B (complex V; Invitrogen). Immunoblot detection of the respiratory supercomplex was performed using mitochondria solubilized with 1% (w/v) digitonin. The same amount of pooled mitochondrial protein from control subjects ($n = 10$) was used as the control. The primary antibodies used were as follows: 0.02 $\mu\text{g/ml}$ anti-SDHA (complex II; Invitrogen) and 2 $\mu\text{g/ml}$ anti-UQCRC1 (CIII; Abcam). The band intensity of the supercomplex was estimated by densitometry and normalized to that of complex II. The data were obtained by three independent assays.

Results

Patient 1 (V:2 in Fig. 1A) is a Hispanic female born to a 26-year-old healthy female (G2P2Ab0) and a 28-year-old healthy male who are second cousins. She was delivered at 37 weeks by Cesarean section because of a pathological cardiotocogram. At birth, she weighed 2,329 g (5–10th percentile) with a length of 46 cm (5–10th percentile), and her occipitofrontal circumference was 34 cm (25–50th percentile). Her Apgar scores were 8, 9, and 9 at 1, 5, and 10 min, respectively. She developed a severe metabolic acidosis

(pH 7.1, with a base excess of -24.6 mEq/l) within 1 day, requiring admission to a neonatal intensive care unit. Blood lactate and pyruvate on admission were 25.5 mM (reference range: <2.2 mM) and 0.436 mM (reference range: <0.16 mM), respectively (lactate to pyruvate ratio = 58.48). Clinical examination revealed tachypnea (47 breaths/min), tachycardia (181 beats/min), mild subcostal retractions, Levine II/VI systolic cardiac murmur, no organomegaly, and poor sucking reflex. Blood ammonia was 126 μM (reference range in neonates: <80 μM). The patient responded promptly to supportive therapy, with intravenous glucose infusion providing 10 mg/kg/min and a sodium bicarbonate drip improving the blood lactate level down to 12.7 mM within 24 hr. The lactate and pyruvate levels further improved to 3.1 and 0.125 mM within 3 days, respectively. Urine organic acid analysis on admission was remarkable for massive lactic and pyruvic aciduria, as well as ketonuria. Plasma amino acids were remarkable for a high alanine level (1,519 μM ; reference range: 200–600 μM). Magnetic resonance imaging (MRI) of the brain revealed small right parietal and temporal infarcts.

She recovered without sequelae and was discharged on full oral feeds with a high-carbohydrate, reduced-fat formula (60% of calories from carbohydrate, 30% of calories from fat) after 1.5 months of hospitalization. She was also diagnosed with an atrial septal defect and renal tubular acidosis. After the initial hospitalization, she was hospitalized more than 10 times because of episodic metabolic decompensation with lactic acidosis (highest value was 10.8 mM at the age of 3 years and 10 months), hyperammonemia (highest value was 346 μM at the age of 3 years and 3 months), ketosis, and hypoglycemia, which were triggered by intercurrent illnesses including fevers, vomiting, and diarrhea. The patient is now 5 years of age, with normal growth and no signs of intellectual disability. The frequency of hospitalization has decreased, although she still requires urgent medical treatment with intravenous glucose infusion to prevent metabolic decompensation during intercurrent illnesses.

Patient 2 (V:3 in Fig. 1A) is a younger full sibling of patient 1. He was born at 39 weeks of gestation by repeat Cesarean section. At birth, he weighed 2,658 g (5–10th percentile) with a length of 49 cm (25–50th percentile), and his occipitofrontal circumference was 34.3 cm (25th percentile). His Apgar scores were 8 and 9 at 1 and 5 min, respectively. He developed tachypnea, grunting, and poor feeding within 1 day because of lactic acidemia. The initial capillary blood gas showed a pH of 7.05, $p\text{CO}_2$ of 25 mmHg, bicarbonate of 5.8 mmol/l, and a base excess of -22 mEq/l. He was intubated for 2 days and treated with intravenous glucose infusion and a bicarbonate drip to correct the metabolic acidosis. Feeding with a high-carbohydrate, reduced-fat formula was started in 10 days. His initial hospitalization was 1-month long, during which he was diagnosed with congenital lactic acidemia and persistent hypoglycemia of unknown etiology. He was treated with corticosteroid replacement therapy owing to adrenal insufficiency for 4 months until a normal adrenocorticotropic hormone stimulation test was obtained. At the age of 8 months, he was found unresponsive after 6 hr of fasting owing to decreased appetite associated with a 2-day mild upper-respiratory-tract infection. At a local emergency room, metabolic acidosis (pH 7.23), hypoglycemia (3 mg/dl; reference range: >60 mg/dl), and hyperammonemia (463 μM), as well as ketosis (blood and urine), were noted. He had five episodes of generalized seizure associated with this episode. Following treatment with levetiracetam, he has been seizure free. Brain MRI findings at the age of 8 months were unremarkable. He was hospitalized for 1 month and discharged without sequelae, and had more than 10 hospitalizations because of similar episodes of lactic acidosis, hypoglycemia, hyperammonemia, and ketosis triggered by intercurrent illnesses. Developmental delay was noted once at 4 months of age. Following

physical and speech therapy, his development was later evaluated as normal at 3 years of age. He is now 4 years of age, with normal growth and no signs of intellectual disability. Physical examination revealed neither dysmorphic features nor abnormal focal neurological signs. He has been fed with a reduced-fat, high-carbohydrate diet and fasting precautions. The frequency of hospitalization has decreased, although he continues to require urgent medical treatment with intravenous glucose infusion to prevent metabolic decompensation during intercurrent illnesses. Laboratory study data obtained in the acute severe metabolic decompensation stage at 16 months of age were remarkable, which are as follows: pH 7.19 capillary blood gas, 11 mg/dl glucose, 348 μ M blood ammonia, and 6.8 mM blood lactate. Urine organic acid analysis showed markedly elevated 3-hydroxybutyrate and acetoacetate indicating severe ketosis, markedly elevated lactate and pyruvate indicating lactic acidosis, markedly elevated dicarboxylic acids (adipic acid, 1,194 mmol/mol Cr [reference range: <15 mmol/mol Cr], suberic acid, 122 mmol/mol Cr [reference range: <7 mmol/mol Cr], sebacic acid, 288 mmol/mol Cr [reference range: <2 mmol/mol Cr]) indicating hyperactive fatty acid beta oxidation, and moderately elevated tricarboxylic acid cycle intermediates including malate, fumarate, and 2-oxoglutarate. Plasma amino acids showed elevated alanine at 440 μ M (reference range: 23–410 μ M). Acylcarnitine profiles obtained at 19 months of age in mild decompensation showed marked elevation of C2 (48 nmol/ml [reference range: 2.6–15.5 nmol/ml]) and moderate elevation of 3-hydroxyacylcarnitines (C12–C18).

Patient 3 (VI:1 in Fig. 1A) is a girl born to consanguineous parents within the same pedigree as patients 1 and 2, but in a different branch. She was small for gestational age and was born vaginally to a 23-year-old mother after a full-term gestation. Her birth weight was 2,200 g. Initially, she had mild respiratory distress and required 1 additional day of monitoring. By 18 months of age, she had undergone four hospitalizations for vomiting, dehydration, and hypoglycemia. An initial blood examination at 18 months of age showed that her blood glucose was 17 mg/dl, bicarbonate was 8 mmol/l, and anion gap was 30 mmol/l. The simultaneous blood lactate and pyruvate levels were 26.3 mg/dl (reference range: <16.0 mg/dl) and 1.5 mg/dl (reference range: <1.5 mg/dl), respectively. She responded quickly to intravenous dextrose with correction of the hypoglycemia and metabolic acidosis. She had developmental delay and microcephaly (second percentile) that led to a brain MRI, but this was interpreted as normal. At 18 months, she spoke only two words but could follow two-part commands. She walked at 15 months of age and had low body weight until starting occupational therapy at 14 months of age. She was not dysmorphic. Her muscle strength and tone were normal when she was in good health, allowing her to climb, hop, and jump in a manner appropriate for her age.

Considering the consanguinity in this family, we hypothesized that the disease was inherited in an autosomal recessive fashion. Linkage analysis using two patients (1 and 2) and three unaffected family members (IV:1, IV:2, and V:1) indicated that homozygous regions totaling 36-Mb were shared by the two affected individuals with logarithm of the odds scores ≥ 2.0 , as calculated by Allegro version 2 [Gudbjartsson et al., 2005] (Supp. Table S1). We then performed whole-exome sequencing of DNA from patient 1. Two homozygous variants within the 36-Mb homozygous regions were identified: c.547C>T, p.Arg183Trp in *UQCRC2* (NM_003366) and c.1675A>G, p.Met559Val in *TNRC6A* (NM_014494). Sanger sequencing confirmed the two variants in patient 1. The Polyphen-2 program (<http://genetics.bwh.harvard.edu/pph2/>) predicted that p.Arg183Trp in *UQCRC2* and p.Met559Val in *TNRC6A* were probably damaging and benign, respectively (Table 1). *TNRC6A* was

Table 1. Prediction of Mutational Effects in UQCRC2

Mutation	Alteration	Type	Grantham score ^a	Polyphen-2	Energy ddG ^b
c.547C>T	p.Arg183Trp	Mutant	101	0.998	10.02
c.548G>A	p.Arg183Gln	SNP	43	0.177	2.19
c.547_548CG>AA	p.Arg183Lys	Ortholog	26	0.001	1.74

^aGrantham score indicates the chemical dissimilarity caused by codon replacements.

^bThe corrected average interaction energy ddG of each altered amino acid is calculated by FoldX as homozygous mutation.

ruled out as a candidate because the heterozygous *TNRC6A* change was found in patient 3. *UQCRC2* encodes ubiquinol–cytochrome c reductase core protein II (UQCRC2; MIM# 191329), a core protein of CIII. All three patients possessed the homozygous p.Arg183Trp change in *UQCRC2*, whereas the father (IV-2), mother (IV-1), and sister (V-1) (all unaffected) were heterozygous (Fig. 1B). This change was not observed among 80 Mexican control alleles or 750 Japanese control alleles.

To predict the effect of the missense mutation (c.547C>T, p.Arg183Trp) on the structural stability of CIII, we calculated the free-energy change of interactions between the core protein monomers (encoded by *UQCRC2*) with and without the mutation using FoldX software (version 3.0) [Guerois et al., 2002; Khan and Vihinen, 2010]. For this calculation, we used the crystal structure of bovine CIII (PDB code 2A06) as a structural model because no crystal structure is available for human UQCRC2. Amino acid position 183 of UQCRC2 is a highly conserved basic amino acid among species from zebrafish to humans (e.g., Arg in humans and cows, Lys in mice; Fig. 1C) and is reported to be substituted for Gln as a nonsynonymous human SNP (rs4850 [c.548G>A, p.Arg183Gln]) (Fig. 1C). Therefore, we also calculated the interaction-energy change upon replacement of Arg183 with Lys or Gln, in addition to the Trp found in the patient. The calculated interaction-energy change caused by replacement of Arg183 with Trp was estimated as 10 kcal/mol, whereas those caused by replacement with Lys or Gln were no more than 2 kcal/mol (Fig. 2A, Table 1). The molecular structure of the wild-type core protein homodimer indicated that the methylene part of the Arg183 side chain of one subunit forms a hydrophobic core with the side chains of His254 and Phe449 of the other subunit at the homodimer interface (Fig. 2B and C). When the Arg183 of the core protein was replaced by Trp, the introduced Trp183 side chain flipped outward from the original side-chain position because of steric hindrance (Fig. 2D). In contrast, when Arg183 was replaced by Lys or Gln, each side chain occupied the original position to maintain a hydrophobic core with the methylene part of Lys or Gln (Fig. 2E and F). This indicates that the Arg183Trp mutation in *UQCRC2* would disrupt the hydrophobic core formed at the interface of the UQCRC2-containing complex, resulting in destabilization of CIII. In vitro experiments showing that the exogenous and endogenous expressions of the UQCRC2 mutant were significantly reduced (Supp. Figs. S1 and S2) may support the protein instability.

To test whether this mutation alters UQCRC2 localization at the mitochondrial inner membrane, we created mammalian full-length wild-type, mutant, and SNP (rs4850) constructs; transiently overexpressed them in COS1 cells; and observed their localization microscopically. The mutant protein colocalized with mitochondria, similar to the wild-type and SNP proteins (Supp. Fig. S3). This indicates that the p.Arg183Trp mutation probably does not alter the intracellular localization.

To evaluate mitochondrial function in vitro, we measured the enzyme activities of the mitochondrial respiratory chain complexes